Reactivity and redox potential of hole localization in liquid water

Francesco Ambrosio* and Alfredo Pasquarello

Chaire de Simulation à l'Echelle Atomique (CSEA), Ecole Polytechnique Fédérale de Lausanne (EPFL), CH-1015 Lausanne, Switzerland

E-mail: Francesco.Ambrosio@epfl.ch

Phone: +41 21 6933423. Fax: +41 21 693 5419

*To whom correspondence should be addressed

Abstract

We study the reactivity and the redox potential associated with the reduction of the $H_2O^{\bullet+}$ radical cation in liquid water by combining *ab initio* molecular dynamics simulations at the hybrid functional level, a grand-canonical formulation of solutes in aqueous solution, and nudge-elastic-band calculations. We demonstrate that this extremely oxidative solute promptly dissociates and calculate an energy barrier for the reaction of 0.06 eV, consistent with the short measured lifetimes. We calculate the $H_2O^{\bullet+}/H_2O$ redox level with respect to the vacuum level and to the computational standard hydrogen electrode (SHE), using the thermodynamic integration method. The calculated $H_2O^{\bullet+}/H_2O$ redox level lies at 3.8±0.1 eV above the SHE level, in remarkable agreement with the experimental estimate. The implications of the present results for the mechanism of water splitting at the heterogenous semiconductor-water interface are discussed.

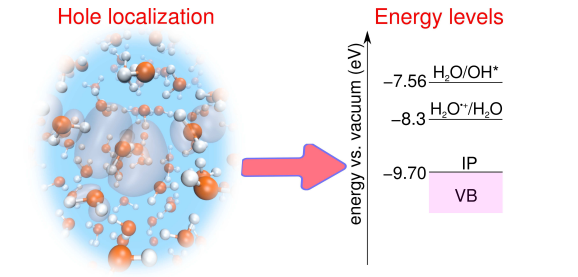

Reaction and redox level of hole capture in liquid water from first principles

Graphical Table of Contents

1 Introduction

The physics of excess electrons and holes in liquid water is quintessential for understanding the redox chemistry and the response to light and ionizing radiations of aqueous solutions, as these properties are related to phenomena which are relevant to various fields, ranging from radiotherapy to photocatalysis.[1,2] While the physics of localized electrons in liquid water has

been extensively studied, from both the structural and thermodynamical point of view,[3–11] the localized hole in the liquid has been more elusive.

It is known that, upon ionization, an excess hole rapidly localizes on a single water molecule, forming the highly-reactive radical $H_2O^{\bullet+}$:[12–14]

$$H_2O(\ell) + h^+ \rightarrow H_2O^{\bullet+}(aq). \tag{1}$$

From both the experimental and theoretical point of view, the determination of the redox potential associated to the reaction of Eq. (1) is hindered by the extremely short lifetime ($\sim$200 fs) of the $H_2O^{\bullet+}$ radical cation.[12] In fact, this strongly oxidizing species is also highly acidic and promptly looses a proton to a neighboring water molecule:

$$H_2O^{\bullet+}(aq) + H_2O(\ell) \rightarrow OH^{\bullet}(aq) + H_3O^+(aq). \tag{2}$$

This reaction is thought to occur through a cationic dimer complex $H_4O_2{}^{\bullet+}$.[12,15,16] In this framework, theoretical studies are mostly limited to small clusters.[12,15,17–26]

In particular, the water dimer has been largely investigated, as the simplest model to study the water cation and its reactivity.[15,17,18,21,25,26] Studies based on coupled-cluster theory have shown that, upon injection of the hole in the dimer, proton transfer occurs within 50 fs for ionization to the electronic ground state of $H_2O^{\bullet+}$.[15,18] Similar results have also been achieved using density functional theory calculations at the hybrid functional level, thus suggesting that this level of theory may be used to study larger systems that are computationally prohibitive for post-Hartree Fock methods.[17,20,21,26] Similar dynamics of proton dissociation have been observed in larger water clusters.[19,22] However, upon increasing the size of the cluster to more than four molecules, a different mechanism has become apparent, in which the solvation of the hydronium cation becomes the dominant driving force of the reaction.[23,24] In particular, the study of clusters up to 21 water molecules indicates that the separation between the hydroxyl radical and the hydronium cation is fundamental for the

stability of the system, as these two moieties are found to be at the opposite ends of the clusters upon relaxation of the ionized system.[24]

Only few *ab initio* simulations have been performed accounting explicitly for the molecular liquid, and the effect of using approximated density functionals[27] has poorly been investigated. The current determination of the redox level is even more vague. Ma *et al.* have inferred from measured and theoretical thermodynamical data that the redox potential of the $H_2O^{\bullet+}/H_2O$ couple should be about 4 eV vs. the standard hydrogen electrode (SHE) but invoked the need of more accurate simulations for achieving better estimates.[13]

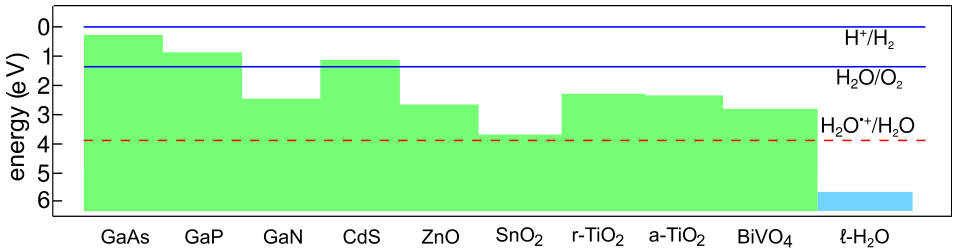

Figure 1: Valence band edge of GaAs, GaP, GaN, CdS, ZnO, SnO_2, TiO_2 (rutile and anatase), and $BiVO_4$ in aqueous environment at their respective pH_{PZC} (from Refs. 28,29), compared with the current experimental estimate for the $H_2O^{\bullet+}/H_2O$ redox potential (dashed red, from Ref. 13). The redox potentials of water (solid, blue) are also indicated. All energies are referred to the SHE level.

The precise determination of the redox level associated with the reaction of Eq. (1) also has implications in heterogeneous photocatalysis. In fact, photocatalytic water splitting is prompted by holes provided by the valence band edge of a semiconducting material at the interface with liquid water. In particular, from the reactions of Eqs. (1) and (2), we obtain the so-called dehydrogenation reaction, which represents the first step of the water oxidation reaction in acidic conditions:[30]

$$2H_2O(\ell) + h^+ \rightarrow OH^{\bullet}(aq) + H_3O^+(aq). \tag{3}$$

However, from the band-alignment at the semiconductor-water interface (cf. Fig. 1),[28,29] we notice that semiconductors usually employed in photocatalytic water splitting have valence

band edges at much higher energy than the current experimental estimate of the $H_2O^{\bullet+}/H_2O$ redox level.[13] If the position of this level is confirmed, this would imply that the reaction of Eq. (3) with the water radical cation as an intermediate would require the overcoming of high energy barriers, making this mechanism highly improbable.

Thermodynamic energy levels associated to polaronic states in a bulk material are usually calculated from molecular dynamics simulations through the thermodynamic integration of vertical energy differences.[11,31–33] In the case of the $H_2O^{\bullet+}/H_2O$ energy level, two vertical energy differences should be considered, when adopting the Marcus approximation: (i) the vertical ionization energy of liquid water and (ii) the vertical reduction of $H_2O^{\bullet+}$. The calculation of both of these quantities presents challenges that are not commonly encountered when treating solutes in aqueous solution. In particular, the vertical ionization energy of liquid water is related to the absolute position of its valence band edge and an accurate description of this level is consequently required, in order to correctly describe electronic levels lying close to it. On the other hand, the calculation of the vertical reduction of the $H_2O^{\bullet+}$ radical cation is hindered by the fast dissociation of this solute, which impedes an accurate sampling of vertical energy differences. Furthermore, the Marcus approximation may not be sufficient to achieve an accurate thermodynamic integral due to deviations that are often encountered for redox levels involving localization upon electron trasfer.[11,34,35]

In this Article, we study the reduction of the $H_2O^{\bullet+}$ cation combining *ab initio* molecular dynamics simulations at the hybrid functional level, a grand-canonical formulation of solutes in aqueous solution, and nudge-elastic-band calculations. First, we show the rapid localization of the hole on a single water molecule upon ionization. Next, we investigate the dissociation reaction of the $H_2O^{\bullet+}$ radical cation [cf. Eq. (2)]. We show that the reaction occurs through a dimeric $H_4O_2{}^{\bullet+}$ transition state and find an energy barrier of 0.06 eV for the reaction, consistent with the short lifetimes measured for the $H_2O^{\bullet+}$ cation. Then, we calculate the $H_2O^{\bullet+}/H_2O$ redox level with respect to the vacuum level and to the computational standard hydrogen electrode (SHE), by combining molecular dynamics simulations

and the thermodynamic integration method. Our results place the redox potential of the $H_2O^{\bullet+}/H_2O$ couple at 3.8 $\pm$ 0.1 eV vs. SHE, in remarkable agreement with the experimental estimate.

2 Methods

Calculations are performed with the freely available `CP2K` suite of codes,[36] which is based on the use of atomic basis sets and of a plane-wave expansion for the electron density. Norm-conserving Goedecker-Teter-Hutter pseudopotentials[37,38] are used to account for core-valence interactions. Valence electrons of O and H atoms are described with a triple-ζ correlation-consistent polarized basis set (cc-pVTZ).[39] The plane-wave basis set is delimited by a kinetic-energy cutoff of 800 Ry. The sampling of the Brillouin zone is achieved at the Γ point.

All the calculations are performed at the hybrid functional level, using the highly-efficient auxiliary density matrix method[40–42] implemented in `CP2K`. In particular, we employ our recently developed h-rVV10 functional,[43] which is a hybrid exchange-correlation functional including nonlocal van der Waals (vdW) interactions. In this scheme, the fraction α of Fock exchange in the PBE0 functional[44,45] is optimized in conjunction with the b parameter, which governs the extent of the short-range vdW interactions in the rVV10 formulation,[46,47] in order to reproduce the structural and electronic properties of liquid water.[43] The optimized functional with $\alpha = 0.40$ and $b = 5.3$ has also proved to be remarkably accurate in describing the energetics of water clusters, different phases of ice, aqueous solutions, and water-semiconductors interfaces.[43,48] In this work, we further benchmark the accuracy of the h-rVV10 functional for aqueous systems, by studying the energetics of the two main isomers of the water dimer cation $(H_2O)_2^+$: (i) the proton-transferred and (ii) the hemibonded structure (cf. Fig. 2). While accurate calculations at the coupled cluster level of theory including single, double, and triple excitations [CCSD(T)] indicate that the proton-transferred struc-

ture is more stable than the hemibonded one by as much as 0.38 eV (cf. Table 1),[16] semilocal functionals have been shown to give an opposite outcome.[17,20] This failure is attributed to the noxious self-interaction error affecting semilocal density functional approximations,[49] which is particularly dramatic for systems including unpaired electrons.[50] However, while hybrid functionals have shown to qualitalively reproduce the correct ordering, the quantitative agreement with the CCSD(T) benchmark has been found to be erratic, with large differences among different functionals.[20]

We here test our h-rVV10 functional by calculating the relative energy of the two dimer structures $E_{\rm rel} = E_{\rm hemi} - E_{\rm pt}$, where $E_{\rm hemi}$ and $E_{\rm pt}$ are the total energies of the hemibonded and proton-transferred dimer, respectively. The h-rVV10 functional (cf. Table 1) gives $E_{\rm rel} =$ 0.30 eV, only 0.08 eV below the CCSD(T) reference and in line with the best estimates reported for other hybrid functionals.[20] In order to assess the role of vdW interactions, we also calculate $E_{\rm rel}$ at the PBE0(0.40) level, and we observe almost no difference with respect to the h-rVV10 results. In contrast, when compared to previous results at the standard PBE0 level (i.e. with $\alpha = 0.25$), we remark that the increased fraction of Fock exchange in our functionals noticeably improves the agreement with the CCSD(T) reference. This observation is consistent with previous works showing that a large fraction of Fock exchange is needed to accurately simulate cationic clusters of water molecules.[20]

Table 1: $E_{\rm rel}$ (eV) at various levels of theory.

Theory	$E_{\rm rel}$
Reference: CCSD(T)[16,20]	0.38
PBE0[20]	0.11
PBE0(0.40)	0.31
h-rVV10	0.30

For the condensed-phase simulations, we consider an atomistic model of liquid water consisting of 64 water molecules in a periodic supercell with a side of $L = 12.42$ Å, corresponding to the experimental density.[43] We carry out Born-Oppenheimer molecular dynamics simulations in the NVT ensemble with a Nosé-Hoover thermostat[51,52] with a target temperature

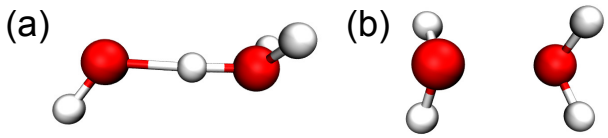

Figure 2: Representation of (a) the proton-transferred and (b) the hemibonded water dimer cation $(H_2O)_2^+$. O atoms in red, H in white.

T =300 K and a time constant of the thermostat chain set at 16.68 fs. A time-step of 0.48 fs is employed and individual simulations are continued for 5-10 ps.

3 Results and discussion

We first perform perform ten *ab initio* molecular dynamics simulations of liquid water with an extra hole starting from configurations achieved with a previous MD run of neutral liquid water.[43] The starting configurations are equally spaced in time by 1 picosecond. In all cases, we observe rapid dissociation of a water molecule according to the reaction of Eq. (2). From the ten MD runs, we estimate an average reaction time of ∼50 fs, in line with a previous theoretical study.[27] Furthermore, the products of the reaction, H_3O^+(aq) and $OH^\bullet$(aq), which are initially close to each other separate completely within ∼250 fs of simulation. We note that, similarly to Ref. 27, our dissociation time is underestimated with respect to the experiment,[12] because we consider only ionization to the electronic ground-state of $H_2O^{\bullet+}$. It has been shown in cluster studies that proton transfer can be up to four times slower when excited states are involved, due to a reduced localization of the positive charge on the hydrogen atoms.[15,18]

To get deeper insight into the mechanism and the energetics of the reaction, we perform a nudge-elastic-band calculation (NEB) between a starting configuration in which the hole is injected in a bulk-like configuration and a final configuration in which $OH^\bullet$ and H_3O^+ are formed upon proton transfer. NEB calculations at the h-rVV10 level are perfomed with the improved tangent (IT) method,[53] considering nine replicas between the initial and final

configurations. In the NEB calculations, only the atoms belonging to the two water molecules involved in the reaction are allowed to relax while the other atoms are frozen in their initial configuration, in order to avoid the convergence problem arising from the relaxation of the full aqueous system to 0 K. This is justified by the short timescales of the reaction observed in the MD simulations, over which no significant rearrangement of the surrounding water molecules occurs. To correctly sample the saddle point observed in the NEB calculation, we carry out a second NEB with 7 replicas between the structure corresponding to the first minimum and that associated to the first point after the maximum. We observe a negligible variation of the barrier (<0.01 eV) upon such a refinement of the sampling close to the saddle point.

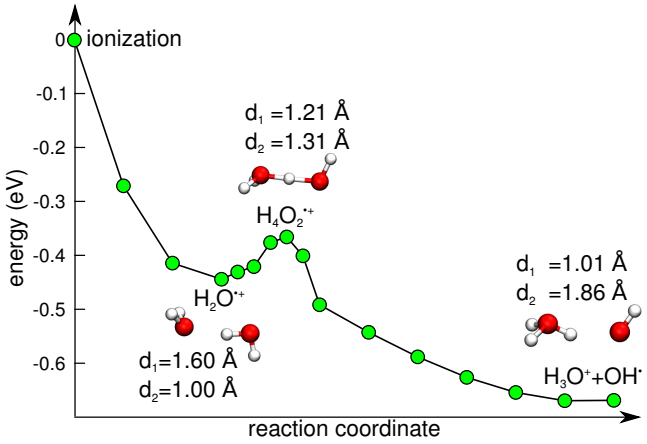

Figure 3: Energy diagram illustrating the process of hole localization and successive proton transfer along the reaction coordinate. A schematic representation of the reaction intermediates is reported along with the O-H distances between the oxygen of the involved water molecules and the proton undergoing transfer.

The analysis of the NEB calculations (cf. Fig. 3) allows us to understand in detail the reaction mechanism. Upon vertical ionization, the injected positive charge is delocalized on a large fraction of water molecules of the supercell (cf. Fig. 4). This is consistent with the electron being extracted from the partially delocalized valence band edge of liquid water, in line with previous calculations at the hybrid functional and *GW* levels.[34,54] Furthermore, partial delocalization of the hole upon ionization has also been observed in *ab initio* studies on large clusters.[55–57] Then, the hole rapidly localizes on an O $2p$ orbital of a single water

molecule (cf. Fig. 4) with an energy gain of ∼0.45 eV, thus forming the $H_2O^{\bullet+}$ radical. In our ten MD simulations, the hole always localizes on a water molecule which presents a lower number of accepted hydrogen bonds than on average. Formation of the $H_2O^{\bullet+}$ is accompanied by a 0.1 Å elongation of the O-H bonds and a decrease of the H-O-H angle by 5°. The highly acidic $H_2O^{\bullet+}$ radical cation promptly dissociates through a dimeric transition state ($H_4O_2{}^{\bullet+}$) in which a proton is shared between two water molecules (cf. Fig. 4). From the NEB calculations, we estimate an energy barrier of 0.06 eV for this acid-base reaction (cf. Fig. 3), smaller than the barrier of 0.13 eV recently estimated for proton transfer of the aqueous proton.[58]

In our ground-state picture of the process, we employ transition state theory, to define the lifetime τ of the $H_2O^{\bullet+}$ radical cation as follows:

$$\frac{1}{\tau} = \nu_{\mathrm{OH}} e^{-\Delta E/k_{\mathrm{B}}T} \tag{4}$$

where ν_{OH} is the frequency of the OH stretching in liquid water, ΔE is the calculated energy barrier, k_{B} the Boltzmann constant, and T the temperature. We consider ν_{OH} since the reaction follows a reaction coordinate defined along the $O_{wc}-H-O_w$ path, where O_{wc} and O_w are the oxygen atoms of the cation and of the water molecules receiving the proton, respectively. Furthermore, during the MD simulations, we observe a few oscillations of the proton shared in the cationic dimer complex $H_4O_2{}^{\bullet+}$. Taking $\nu_{\mathrm{OH}} = 3404$ cm^{-1},[59] we obtain $\tau = 108$ fs at 300 K, consistent with lifetimes measured through polarization anisotropy experiments (198 fs).[12] Hence, the experimental lifetimes are slightly larger than the estimates inferred from transition state theory. This could be due to the fact that our description accounts neither for excited states, which are found to reduce the acidity of the water cation,[18] nor for nuclear quantum effects, which enhance the delocalization of the protons.[60] The oscillations of the proton observed for the cationic dimer complex $H_4O_2{}^{\bullet+}$ in the MD simulations indicate that in our ground-state picture the ionized molecule does not

acquire a large excess energy upon vertical ionization of the system. This is also confirmed by the fact that the temperature in the initial stages of the simulation remains close to the target temperature of the thermostat. Therefore, the use of a temperature of 300 K in Eq. (4) is justified. In the last step of the reaction, an energy gain of ∼0.3 eV is observed upon dissociation of $H_2O^{\bullet+}$ (cf. Fig. 3). It should be noted that an extra stabilization of ∼0.7 eV is calculated upon complete separation between the hydronium cation and the hydroxyl radical, with the formation of two distinct solvation shells for the solutes.[34]

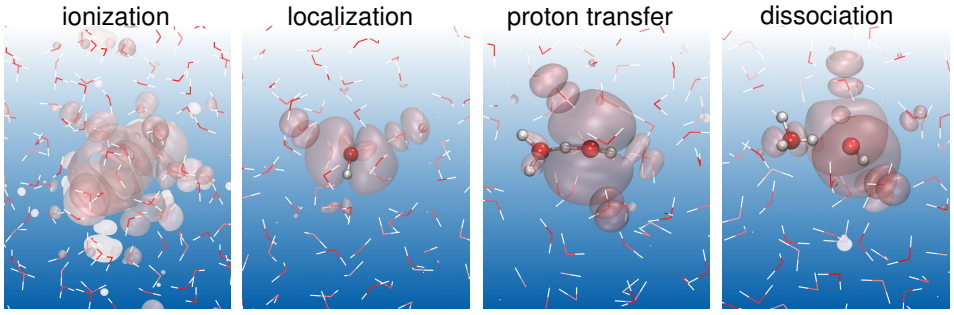

Figure 4: Isodensity representation of the hole wave function (i) upon vertical injection, (ii) after localization on a single water molecule, (iii) during and (iv) after proton transfer.

Next, we calculate the redox level associated with the reduction of the $H_2O^{\bullet+}$ cation. The species studied in this work is indeed short-lived and, therefore, thermodynamic electronic properties such as charge transition levels[61–63] and redox levels[34] cannot directly be defined in principle. However, by sampling the local minimum associated with the $H_2O^{\bullet+}$ cation, we can estimate its redox properties by applying the grand-canonical formulation of solutes in aqueous solution, recently employed to calculate redox levels in aqueous solution.[34,64] Free energy differences are defined through the use of a fictitious Hamiltonian $\mathcal{H}_\eta$:

$$\mathcal{H}_\eta = \eta\mathcal{H}_{\text{hole}} + (1-\eta)\mathcal{H}_{\text{H}_2\text{O}(\ell)}, \tag{5}$$

which connects the Hamiltonian of the reactant $H_2O(\ell)$ with that of the product $H_2O^{\bullet+}$ via the Kirkwood coupling parameter $0 \leq \eta \leq 1$.[65] In this work, mixed systems are generated by mixing the forces achieved from self-consistent calculations of the neutral and the positively

charged system.[36] In this formulation, we obtain the following expression for the adiabatic redox level $\mu_{\rm hole}$:

$$\mu_{\rm hole} = \int_0^1 \langle \Delta E_{\rm ox} \rangle_\eta d\eta - \epsilon_{\rm v} = \Delta_{\rm ox} A_{\rm H_2O^{\bullet+}} - \epsilon_{\rm v}, \tag{6}$$

where $\langle \Delta E_{\rm ox} \rangle_\eta$ corresponds to vertical energy differences for structural configurations achieved at various values of η, $\epsilon_{\rm v}$ is the valence band edge of liquid water, and $\Delta_{\rm ox} A_{\rm H_2O^{\bullet+}}$ is the thermodynamic integral associated to the oxidation of the water cation. In the proposed theoretical framework, $\langle \Delta E_{\rm ox} \rangle_{\eta=0}$ corresponds to the average of vertical ionization energies, i.e. the total-energy difference achieved upon vertical injection of a hole in the system. At variance, $\langle \Delta E_{\rm ox} \rangle_{\eta=1}$ is defined as an average vertical reduction energy, achieved by vertically introducing a single electron in the system containing a $H_2O^{\bullet+}$ radical cation. Fractional values of η represent molecular dynamics simulations evolving through forces obtained from $\mathcal{H}_\eta$. In this work, we employ three fractional values of η (0.1, 0.25, 0.5) in order to achieve an accurate estimate of the thermodynamic integral. The calculated energy levels are aligned with respect to (i) the computational standard hydrogen electrode (SHE)[34,35] and (ii) to the vacuum level using an atomistic description of the water-vacuum interface.[66]

Our MD simulations show that the calculation of $\langle \Delta E_{\rm ox} \rangle_{\eta=0}$ corresponds to the sampling of the delocalized valence band edge (cf. Fig. 4). The position of such a delocalized state can largely depend upon the employed electronic structure method.[34] For this reason, to estimate $\langle \Delta E_{\rm ox} \rangle_{\eta=0}$ we employ the value of the valence band edge achieved at the PBE0(α) level, in which the fraction of Fock is fixed at 0.45, following the rationale employed in Ref. 66. In this way, the valence band edge of liquid water is placed at 9.70 $\pm$ 0.05 eV (error calculated by blocking analysis[67]) below the vacuum level, in remarkable agreement with the available experimental range for the ionization potential of liquid water, comprised between -9.3 and -10.1 eV.[68–71] We also notice that in Ref. 66 the linear extrapolation of the wing of the valence band is used to calculate the ionization potential rather than vertical total-energy differences. However, the two methods have been found to provide equivalent results for the valence band edge of liquid water, when total energy differences are linearly extrapolated to

infinite supercell size.[34]

The vertical energy gaps calculated for the MD simulation carried out at $\eta = 0.1$ still correspond to the sampling of the delocalized valence band edge. Therefore, we consider $\langle \Delta E_{\rm ox} \rangle_{\eta=0} = \langle \Delta E_{\rm ox} \rangle_{\eta=0.1}$. At variance, for η =0.25, 0.5, and 1, we encounter localized defect states within the band gap of liquid water. The energy levels associated to those states do not sensitively depend upon the employed density functional, in analogy to defect levels in the band gap of semiconductors and insulators.[34,61] We verify this by performing calculations with two different values of the fraction of Fock exchange α in the h-rVV10 functional (0.40 and 0.45) for $\langle \Delta E_{\rm ox} \rangle_{\eta=1}$, and finding differences smaller than 0.03 eV. We observe that the calculation of $\langle \Delta E_{\rm ox} \rangle_{\eta=1}$ is hindered by the fact that the $H_2O^{\bullet+}$ radical cation rapidly dissociates after its formation. For this reason, vertical energy differences are calculated on top of a molecular dynamics simulation, in which the coordination numbers of all O atoms of the water molecules are constrained through harmonic restraining potentials, as in Ref. 34. In contrast, for $\eta = 0.25, 0.50$, we do not observe water dissociation even in the absence of constraining potentials and despite the large localization on a single water molecule. The calculated vertical energy differences are found to be consistent with $\langle \Delta E_{\rm ox} \rangle_{\eta=1}$ with constraining potentials applied (cf. Fig. 5), thereby providing confidence that such potentials do not affect the achieved result. Furthermore, the restraining potentials are applied to both the oxidized and the reduced systems for consistency and their effect on the calculated redox levels in aqueous solution thus cancels to a large extent.[34,72]

In Fig. 5, we provide the values of $\langle \Delta E_{\rm ox} \rangle$ for each sampled η. We notice that we do not include here any electrostatic finite-size correction for each point corresponding to a localized defect state (i.e. η =0.25, 0.5, 1). In fact, it has been shown that the finite-size correction can be added *a posteriori* on the thermodynamic integral $\Delta_{\rm ox} A_{H_2O^{\bullet+}}$.[34] This correction amounts to 0.03 eV, when adopting the scheme proposed by Freysoldt, Neugebauer, and Van de Walle[73,74] for the supercell with 64 water molecules employed in this work.[34] However, finite-size effects are more significant when focusing on the vertical reduction energy of the water

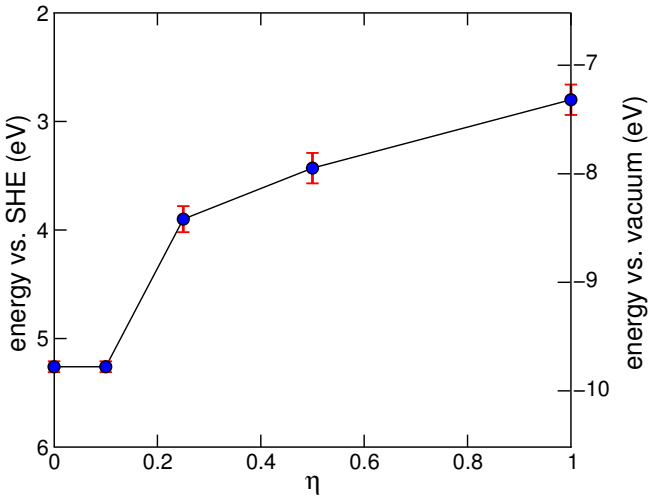

Figure 5: $\langle \Delta E_{\mathrm{ox}} \rangle$ with respect to the SHE and the vacuum level for different values of the Kirkwood parameter η. Errors on each value of $\langle \Delta E_{\mathrm{ox}} \rangle$ are calculated with a blocking analysis and reported in the figure in red.

radical cation:

$$\mu_{\mathrm{ver}} = \langle \Delta E_{\mathrm{ox}} \rangle_1 - \epsilon_{\mathrm{v}}. \tag{7}$$

In this case, the finite-size correction amounts to 0.75 eV and is calculated from a linear extrapolation of $\langle \Delta E_{\mathrm{ox}} \rangle_1$ to a cell of infinite size, after performing a MD simulation including 128 water molecules ($L = 15.64$ Å).[11] Thia gives a value of μ_{ver} at 8.00±0.12 eV below the vacuum level.[11]

The integration of the curve illustrated in Fig. 5 (b) allows us to place μ_{hole} at 3.8 ±0.1 eV below the vacuum level [cf. Fig. 6], where the error on the integral is estimated by considering the minimum and the maximum values of the integral that are achieved when the errors on the individual values of $\langle \Delta E_{\mathrm{ox}} \rangle$ are accounted for. Alternatively, we can align values of $\langle \Delta E_{\mathrm{ox}} \rangle$ with respect to the vacuum level, following Ref. 66 [cf. Fig. 6]. Both alignment schemes produce results in excellent agreement with the experimental characterization, as we calculate μ_{hole} at 3.8 eV vs. SHE and at −8.3 eV vs. vacuum, to be compared with the respective experimental values at 4.03 and −8.47 eV.[13] It should be noted that the position of the valence band edge only slightly influences the calculated thermodynamic integral, at variance with the more sensitive relationship between the redox level of the hydrated electron

and the electron affinity of liquid water.[11] In fact, the curve of Fig. 5 depends upon the value of the valence band edges only up to $\eta = 0.10$. Therefore, the calculated integral changes by less than 0.05 eV when the valence band edge achieved with h-rVV10[43] is used instead of the best available estimate (Ref. 66).

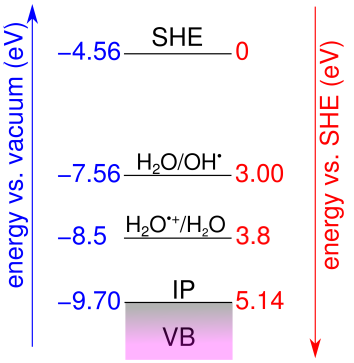

Figure 6: Energy diagram including the IP of liquid water, the $H_2O^{\bullet+}/H_2O$ and $H_2O/OH^{\bullet}$ (from Ref. 34) redox potentials, and the SHE level (from Ref. 66).

The calculated energy level allows us to estimate the acidity of the water cation from the free energy pertaining to the acid-base reaction of Eq. (2). In fact, Eq. (2) is the difference between Eqs. (3) and (1). From Fig. 6, in which the $H_2O/OH^{\bullet}$ redox potential calculated in Ref. 34 is included, we estimate the free energy difference $\Delta G(\mathrm{ab})$ associated to the deprotonation of the aqueous water cation to be 0.8 eV, consistent with the outcome of our NEB and MD calculations. Finally, the acidic constant of the water cation reads as follows:[48]

$$\mathrm{p}K_{\mathrm{a}}[H_2O^{\bullet+}(\mathrm{aq})] = \frac{\Delta G(\mathrm{ab})}{\ln 10 k_{\mathrm{B}} T} - \log c_0, \tag{8}$$

where c_0 is the number of water moles in 1 liter of liquid water (55.5 mol/l). Equation (8) gives $\mathrm{p}K_{\mathrm{a}}[H_3O^{+}(\mathrm{aq})] \cong -14$, thus showing that the water radical cation is far more acidic than even the strongest acids.

The simultaneous oxidizing power and high acidity of the water cation implies that its reactivity may be highly system-dependent.[14] The low lifetime of the species indicates that proton transfer is likely to be dominant in diluted aqueous solutions due to kinetics, even

when electron transfer would be thermodynamically more favourable (cf. Fig. 7). Electron transfer may occur when the water cation is formed close to a hole acceptor (i.e. in biological systems[75] or in concentrated solutions[76]).

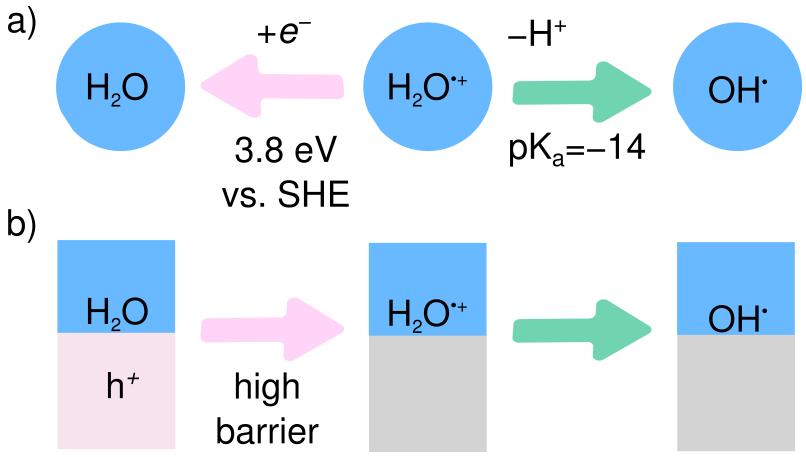

Figure 7: Schematic representation of the (i) the reactivity of aqueous $H_2O^{\bullet+}$ and (ii) possible mechanism of dehydrogenation of the water molecule at the semiconductor-water interface.

The small energy barrier associated with the dissociation of $H_2O^{\bullet+}$ in liquid water indicates a rapid completion of the reaction in Eq. (3) upon hole injection through radiative ionization of liquid water. However, the same reaction with hole localization on a single water molecule at semiconductor-water interfaces would imply overcoming high energy barriers, thus suppressing this mechanism in photocatalytic water splitting (cf. Fig. 7). This can be inferred from Fig. 1, since our work provides a strong confirmation of the available experimental estimate of the redox potential. It is however possible that the interplay with the surface-induced dissociation of water molecules at the semiconductor-water interface may lower this barrier.

4 Conclusions

In conclusion, we studied the reactivity and determined the redox potential of the $H_2O^{\bullet+}$ radical cation in aqueous solution. By combining molecular dynamics simulations and nudge-elastic-band calculations, we calculated an energy barrier of 0.06 eV for the dissociation of this

solute, consistent with the measured lifetimes. The calculated $H_2O^{\bullet+}/H_2O$ redox potential was found at 3.8 ± 0.1 eV vs. the SHE level, in excellent agreement with the experimental characterization. The alignment of the $H_2O^{\bullet+}/H_2O$ energy level at semiconductor-water interfaces typically used for water splitting indicates that the formation of a water radical cation is an unfavourable process and suggests that a different mechanism is operative during the first step of water oxidation.

Acknowledgement

We thank Assil Bouzid and Patrick Gono for fruitful discussions. This work has been performed in the context of the National Center of Competence in Research (NCCR): Materials' Revolution: Computational Design and Discovery of Novel Materials (MARVEL) of the Swiss National Science Foundation. We used computational resources of CSCS and SCITAS-EPFL.

References

(1) Alizadeh, E.; Sanche, L. Precursors of Solvated Electrons in Radiobiological Physics and Chemistry. *Chem. Rev.* **2012**, *112*, 5578–5602.

(2) McKone, J. R.; Lewis, N. S.; Gray, H. B. Will Solar-Driven Water-Splitting Devices See the Light of Day? *Chem. Mater.* **2014**, *26*, 407–414.

(3) Uhlig, F.; Marsalek, O.; Jungwirth, P. Unraveling the Complex Nature of the Hydrated Electron. *J. Phys. Chem. Lett.* **2012**, *3*, 3071–3075.

(4) Marsalek, O.; Uhlig, F.; VandeVondele, J.; Jungwirth, P. Structure, Dynamics, and Reactivity of Hydrated Electrons by Ab Initio Molecular Dynamics. *Acc. Chem. Res.* **2012**, *45*, 23–32.

(5) Uhlig, F.; Herbert, J. M.; Coons, M. P.; Jungwirth, P. Optical Spectroscopy of the

Bulk and Interfacial Hydrated Electron from Ab Initio Calculations. *J. Phys. Chem. A* **2014**, *118*, 7507–7515.

(6) Kumar, A.; Walker, J. A.; Bartels, D. M.; Sevilla, M. D. A Simple ab Initio Model for the Hydrated Electron That Matches Experiment. *J. Phys. Chem. A* **2015**, *119*, 9148–9159.

(7) Turi, L. On the Applicability of One- and Many-Electron Quantum Chemistry Models for Hydrated Electron Clusters. *J. Chem. Phys.* **2016**, *144*, 154311.

(8) Coons, M. P.; You, Z.-Q.; Herbert, J. M. The Hydrated Electron at the Surface of Neat Liquid Water Appears To Be Indistinguishable from the Bulk Species. *J. Am. Chem. Soc.* **2016**, *138*, 10879–10886.

(9) Larsen, R. E.; Glover, W. J.; Schwartz, B. J. Does the Hydrated Electron Occupy a Cavity? *Science* **2010**, *329*, 65–69.

(10) Glover, W. J.; Schwartz, B. J. Short-Range Electron Correlation Stabilizes Noncavity Solvation of the Hydrated Electron. *J. Chem. Theory Comput.* **2016**, *12*, 5117–5131.

(11) Ambrosio, F.; Miceli, G.; Pasquarello, A. Electronic Levels of Excess Electrons in Liquid Water. *J. Phys. Chem. Lett.* **2017**, *8*, 2055–2059.

(12) Li, J.; Nie, Z.; Zheng, Y. Y.; Dong, S.; Loh, Z.-H. Elementary Electron and Ion Dynamics in Ionized Liquid Water. *J. Phys. Chem. Lett.* **2013**, *4*, 3698–3703.

(13) Ma, J.; Schmidhammer, U.; Pernot, P.; Mostafavi, M. Reactivity of the Strongest Oxidizing Species in Aqueous Solutions: The Short-Lived Radical Cation $H_2O^{\bullet+}$. *J. Phys. Chem. Lett.* **2014**, *5*, 258–261.

(14) Ma, J.; Wang, F.; Mostafavi, M. Ultrafast Chemistry of Water Radical Cation, $H_2O^{\bullet+}$, in Aqueous Solutions. *Molecules* **2018**, *23*.

(15) Periyasamy, G.; Levine, R.; Remacle, F. Electronic Wave Packet Motion in Water Dimer Cation: A Many Electron Description. *Chem. Phys.* **2009**, *366*, 129 – 138.

(16) Cheng, Q.; Evangelista, F. A.; Simmonett, A. C.; Yamaguchi, Y.; Schaefer, H. F. Water Dimer Radical Cation: Structures, Vibrational Frequencies, and Energetics. *J. Phys. Chem. A* **2009**, *113*, 13779–13789.

(17) Pieniazek, P. A.; VandeVondele, J.; Jungwirth, P.; Krylov, A. I.; Bradforth, S. E. Electronic Structure of the Water Dimer Cation. *J. Phys. Chem. A* **2008**, *112*, 6159–6170.

(18) Kamarchik, E.; Kostko, O.; Bowman, J. M.; Ahmed, M.; Krylov, A. I. Spectroscopic Signatures of Proton Transfer Dynamics in the Water Dimer Cation. *J. Chem. Phys.* **2010**, *132*, 194311.

(19) Livshits, E.; Granot, R. S.; Baer, R. A Density Functional Theory for Studying Ionization Processes in Water Clusters. *J. Phys. Chem. A* **2011**, *115*, 5735–5744.

(20) Pan, P.-R.; Lin, Y.-S.; Tsai, M.-K.; Kuo, J.-L.; Chai, J.-D. Assessment of Density Functional Approximations for the Hemibonded Structure of the Water Dimer Radical Cation. *Physical Chemistry Chemical Physics* **2012**, *14*, 10705–10712.

(21) Svoboda, O.; Hollas, D.; Ončák, M.; Slavíček, P. Reaction Selectivity in an Ionized Water Dimer: Nonadiabatic Ab Initio Dynamics Simulations. *Phys. Chem. Chem. Phys.* **2013**, *15*, 11531–11542.

(22) Tachikawa, H.; Takada, T. Proton Transfer Rates in Ionized Water Clusters $(H_2O)_n$ $(n = 2 - 4)$. *RSC Adv.* **2015**, *5*, 6945–6953.

(23) Herr, J. D.; Talbot, J.; Steele, R. P. Structural Progression in Clusters of Ionized Water, $(H_2O)^+_{n=1-5}$. *J. Phys. Chem. A* **2015**, *119*, 752–766.

(24) Herr, J. D.; Steele, R. P. Ion-Radical Pair Separation in Larger Oxidized Water Clusters, $(H_2O)^+_n = 6 - 21$. *J. Phys. Chem. A* **2016**, *120*, 7225–7239.

(25) Chipman, D. M. Hemibonding between Water Cation and Water. *J. Phys. Chem. A* **2016**, *120*, 9618–9624.

(26) Chalabala, J.; Uhlig, F.; Slavíček, P. Assessment of Real-Time Time-Dependent Density Functional Theory (RT-TDDFT) in Radiation Chemistry: Ionized Water Dimer. *J. Phys. Chem. A* **2018**, *122*, 3227–3237.

(27) Marsalek, O.; Elles, C. G.; Pieniazek, P. A.; Pluharova, E.; VandeVondele, J.; Bradforth, S. E.; Jungwirth, P. Chasing Charge Localization and Chemical Reactivity Following Photoionization in Liquid Water. *J. Chem. Phys.* **2011**, *135*, 224510.

(28) Guo, Z.; Ambrosio, F.; Chen, W.; Gono, P.; Pasquarello, A. Alignment of Redox Levels at Semiconductor-Water Interfaces. *Chem. Mater.* **2018**, *30*, 94–111.

(29) Ambrosio, F.; Wiktor, J.; Pasquarello, A. pH-Dependent Catalytic Reaction Pathway for Water Splitting at the $BiVO_4$−Water Interface from the Band Alignment. *ACS Energy Lett.* **2018**, *3*, 829–834.

(30) Koper, M. T. M. Theory of Multiple Proton-Electron Transfer Reactions and its Implications for Electrocatalysis. *Chem. Sci.* **2013**, *4*, 2710–2723.

(31) Ambrosio, F.; Wiktor, J.; De Angelis, F.; Pasquarello, A. Origin of Low Electron-Hole Recombination Rate in Metal Halide Perovskites. *Energy Environ. Sci.* **2018**, *11*, 101–105.

(32) Gono, P.; Wiktor, J.; Ambrosio, F.; Pasquarello, A. Surface Polarons Reducing Overpotentials in the Oxygen Evolution Reaction. *ACS Catalysis* **2018**, *8*, 5847–5851.

(33) Wiktor, J.; Ambrosio, F.; Pasquarello, A. Role of Polarons in Water Splitting: The Case of BiVO4. *ACS Energy Lett.* **2018**, *3*, 1693–1697.

(34) Ambrosio, F.; Miceli, G.; Pasquarello, A. Redox Levels in Aqueous Solution: Effect of van der Waals Interactions and Hybrid Functionals. *J. Chem. Phys.* **2015**, *143*, 244508.

(35) Cheng, J.; Sprik, M. Alignment of Electronic Energy Levels at Electrochemical Interfaces. *Phys. Chem. Chem. Phys.* **2012**, *14*, 11245–11267.

(36) VandeVondele, J.; Krack, M.; Mohamed, F.; Parrinello, M.; Chassaing, T.; Hutter, J. Quickstep: Fast and Accurate Density Functional Calculations Using a Mixed Gaussian and Plane Waves Approach. *Comput. Phys. Commun.* **2005**, *167*, 103 – 128.

(37) Goedecker, S.; Teter, M.; Hutter, J. Separable Dual-Space Gaussian Pseudopotentials. *Phys. Rev. B* **1996**, *54*, 1703–1710.

(38) Hartwigsen, C.; Goedecker, S.; Hutter, J. Relativistic separable dual-space Gaussian pseudopotentials from H to Rn. *Phys. Rev. B* **1998**, *58*, 3641–3662.

(39) Dunning, T. H. Gaussian Basis Sets for Use in Correlated Molecular Calculations. I. The Atoms Boron Through Neon and Hydrogen. *J. Chem. Phys.* **1989**, *90*, 1007–1023.

(40) Guidon, M.; Schiffmann, F.; Hutter, J.; VandeVondele, J. Ab Initio Molecular Dynamics Using Hybrid Density F unctionals. *J. Chem. Phys.* **2008**, *128*, 214104.

(41) Guidon, M.; Hutter, J.; VandeVondele, J. Robust Periodic Hartree−Fock Exchange for Large-Scale Simulations Using Gaussian Basis Sets. *J. Chem. Theory Comput.* **2009**, *5*, 3010–3021.

(42) Guidon, M.; Hutter, J.; VandeVondele, J. Auxiliary Density Matrix Methods for Hartree−Fock Exchange Calculations. *J. Chem. Theory Comput.* **2010**, *6*, 2348–2364.

(43) Ambrosio, F.; Miceli, G.; Pasquarello, A. Structrural, dynamical and electronic properties of liquid water: a hybrid functional study. *J. Chem. Phys. B* **2016**, *120*, 7456–7470.

(44) Perdew, J. P.; Ernzerhof, M.; Burke, K. Rationale for Mixing Exact Exchange with Density Functional A pproximations. *J. Chem. Phys.* **1996**, *105*, 9982–9985.

(45) Adamo, C.; Barone, V. Toward reliable density functional methods without adjustable parameters: The PBE0 model. *J. Chem. Phys.* **1999**, *110*, 6158–6170.

(46) Vydrov, O. A.; Van Voorhis, T. Nonlocal van der Waals density functional: the simpler the better. *J. Chem. Phys.* **2010**, *133*, 244103.

(47) Sabatini, R.; Gorni, T.; de Gironcoli, S. Nonlocal van der Waals density functional made simple and efficient. *Phys. Rev. B* **2013**, *87*, 041108.

(48) Ambrosio, F.; Wiktor, J.; Pasquarello, A. pH-Dependent Surface Chemistry from First-Principles: Application to the $BiVO_4$(010)-Water Interface. *ACS Appl. Mater. Interfaces* **2018**, *10*, 10011–10021.

(49) Perdew, J. P.; Zunger, A. Self-Interaction Correction to Density-Functional Approximations for Many-Electron Systems. *Phys. Rev. B* **1981**, *23*, 5048–5079.

(50) Zhang, Y.; Yang, W. A Challenge for Density Functionals: Self-Interaction Error Increases for Systems with a Noninteger Number of Electrons. *J. Chem. Phys.* **1998**, *109*, 2604–2608.

(51) Nosé, S. A Unified Formulation of the Constant Temperature Molecular Dynamics Methods. *J. Chem. Phys.* **1984**, *81*, 511–519.

(52) Hoover, W. G. Canonical Dynamics: Equilibrium Phase-Space Distributions. *Phys. Rev. A* **1985**, *31*, 1695–1697.

(53) Henkelman, G.; Jónsson, H. Improved Tangent Estimate in the Nudged Elastic Band Method for Finding Minimum Energy Paths and Saddle Points. *J. Chem. Phys.* **2000**, *113*, 9978–9985.

(54) Chen, W.; Ambrosio, F.; Miceli, G.; Pasquarello, A. *Ab initio* Electronic Structure of Liquid Water. *Phys. Rev. Lett.* **2016**, *117*, 186401.

(55) Pieniazek, P. A.; Sundstrom, E. J.; Bradforth, S. E.; Krylov, A. I. Degree of Initial Hole Localization/Delocalization in Ionized Water Clusters. *The Journal of Physical Chemistry A* **2009**, *113*, 4423–4429.

(56) Barth, S.; Ončák, M.; Ulrich, V.; Mucke, M.; Lischke, T.; Slavíček, P.; Hergenhahn, U. Valence Ionization of Water Clusters: From Isolated Molecules to Bulk. *J. Phys. Chem A* **2009**, *113*, 13519–13527, PMID: 19856943.

(57) Hartweg, S.; Yoder, B. L.; Garcia, G. A.; Nahon, L.; Signorell, R. Size-Resolved Photoelectron Anisotropy of Gas Phase Water Clusters and Predictions for Liquid Water. *Phys. Rev. Lett.* **2017**, *118*, 103402.

(58) Tahat, A.; Martí, J. Dynamical Aspects of Intermolecular Proton Transfer in Liquid Water and Low-Density Amorphous Ices. *Phys. Rev. E* **2014**, *89*, 052130.

(59) Walrafen, G. E.; Pugh, E. Raman Combinations and Stretching Overtones from Water, Heavy Water, and NaCl in Water at Shifts to ca. 7000 cm^{-1}. *J. Solution Chem.* **2004**, *33*, 81–97.

(60) Marx, D.; Tuckerman, M. E.; Hutter, J.; Parrinello, M. The Nature of the Hydrated Excess Proton in Water. *Nature* **1999**, *397*, 601.

(61) Alkauskas, A.; Broqvist, P.; Pasquarello, A. Defect Energy Levels in Density Functional Calculations: Alignment and Band Gap Problem. *Phys. Rev. Lett.* **2008**, *101*, 046405.

(62) Komsa, H.-P.; Broqvist, P.; Pasquarello, A. Alignment of Defect Levels and Band Edges Through Hybrid Functionals: Effect of Screening in the Exchange Term. *Phys. Rev. B* **2010**, *81*, 205118.

(63) Alkauskas, A.; Broqvist, P.; Pasquarello, A. Defect Levels Through Hybrid Density Functionals: Insights and Applications. *Phys. Status Solidi B* **2011**, *248*, 775–789.

(64) Todorova, M.; Neugebauer, J. Extending the concept of defect chemistry from semiconductor physics to electrochemistry. *Phys. Rev. Appl.* **2014**, *1*, 014001.

(65) Frenkel, D.; Smit, B. *Understanding Molecular Simulation: from Algorithms to Applications*; Academic Press, 2002.

(66) Ambrosio, F.; Guo, Z.; Pasquarello, A. Absolute Energy Levels of Liquid Water. *J. Phys. Chem. Lett.* **2018**, *9*, 3212–3216.

(67) Flyvbjerg, H.; Petersen, H. G. Error Estimates on Averages of Correlated Data. *J. Chem. Phys.* **1989**, *91*, 461–466.

(68) Winter, B.; Weber, R.; Widdra, W.; Dittmar, M.; Faubel, M.; Hertel, I. V. Full Valence Band Photoemission from Liquid Water Using EUV Synchrotron Radiation. *J. Phys. Chem. A* **2004**, *108*, 2625–2632.

(69) Winter, B.; Faubel, M.; Hertel, I. V.; Pettenkofer, C.; Bradforth, S. E.; Jagoda-Cwiklik, B.; Cwiklik, L.; Jungwirth, P. Electronic Binding Energies of Hydrated H_3O+ and OH^-: Photoelectron Spectroscopy of Aqueous Acid and Base Solutions Combined with Electronic Structure Calculations. *J. Am. Chem. Soc.* **2006**, *128*, 3864–3865.

(70) Winter, B.; Faubel, M.; Vácha, R.; Jungwirth, P. Behavior of Hydroxide at the Water/Vapor Interface. *Chem. Phys. Lett.* **2009**, *474*, 241 – 247.

(71) Seidel, R.; Thürmer, S.; Winter, B. Photoelectron Spectroscopy Meets Aqueous Solution: Studies from a Vacuum Liquid Microjet. *J. Phys. Chem. Lett.* **2011**, *2*, 633–641.

(72) Costanzo, F.; Sulpizi, M.; Valle, R. G. D.; Sprik, M. The oxidation of Tyrosine and Tryptophan Studied by a Molecular Dynamics Normal Hydrogen Electrode. *J. Chem. Phys.* **2011**, *134*, 244508.

(73) Freysoldt, C.; Grabowski, B.; Hickel, T.; Neugebauer, J.; Kresse, G.; Janotti, A.; Van de

Walle, C. G. First-principles calculations for point defects in solids. *Rev. Mod. Phys.* **2014**, *86*, 253–305.

(74) Komsa, H.-P.; Rantala, T. T.; Pasquarello, A. Finite-size supercell correction schemes for charged defect calculations. *Phys. Rev. B* **2012**, *86*, 045112.

(75) La Vere, T.; Becker, D.; Sevilla, M. D. Yields of in Gamma-Irradiated DNA as a Function of DNA Hydration: Hole Transfer in Competition with Formation. *Radiation research* **1996**, *145*, 673–680.

(76) Musat, R.; Denisov, S. A.; Marignier, J.-L.; Mostafavi, M. Decoding the Three-Pronged Mechanism of $NO3^{\bullet}$ Radical Formation in HNO_3 Solutions at 22 and 80 °C Using Picosecond Pulse Radiolysis. *J. Phys. Chem. B* **2018**, *122*, 2121–2129.